

A Modified Expectation-Maximization Approach for HMRF-Based Brain MRI Classification

Hussaini Ahmed^{1*}; Jamila Suleiman²; Michael Oluwaseun Dada³;
Omotayo Bamidele Awojoyogbe⁴

¹Federal University of Health Sciences Azare, Bauchi State Nigeria

^{1,2,3,4}Department of Physics, Federal University of Technology, Minna, Niger State, Nigeria

Corresponding Author: Hussaini Ahmed^{1*}

Publication Date: 2025/05/27

Abstract: Accurate segmentation of brain tissues in magnetic resonance imaging (MRI) is essential for clinical diagnosis, pathological assessment, prognosis evaluation, and brain development studies. However, tissue heterogeneity resulting from bias field distortion, partial volume effects, noise, and magnetic field inhomogeneities poses significant challenges. In this study, we propose a Hidden Markov Random Field model combined with a Modified Expectation-Maximization algorithm (HMRF-EM) to improve segmentation accuracy by accounting for neighborhood correlation and signal intensity non-uniformity. The algorithm was implemented in R and evaluated on T1-weighted simulated Brain Web data. The model effectively segmented cerebrospinal fluid (CSF), gray matter (GM), and white matter (WM) with tissue proportions of 35%, 47%, and 18%, respectively. Validation results demonstrated a mean square error of 0.0290, misclassification rate of 0.0870, and tissue volume errors of 0.0578 (CSF), 0.0246 (GM), and 0.0063 (WM). Dice similarity coefficients were 0.9244, 0.9086, and 0.9134 for CSF, GM, and WM, respectively. These findings indicate that the proposed HMRF-EM approach yields reliable and accurate brain tissue classification, making it suitable for clinical and research applications.

Keywords: Magnetic Resonance, Brain Tissue, Segmentation.

How to Cite: Hussaini Ahmed; Jamila Suleiman; Michael Oluwaseun Dada; Omotayo Bamidele Awojoyogbe. (2025). A Modified Expectation-Maximization Approach for HMRF-Based Brain MRI Classification. *International Journal of Innovative Science and Research Technology*, 10(5), 1818-1826. <https://doi.org/10.38124/ijisrt/25may401>.

I. INTRODUCTION

The classification of tissues of brain using magnetic resonance (MR) images is very important for subsequent pathological analysis, diagnosis, prognosis, and following the developmental stage of brain [1]. Thus, Accurate classification is of significance in neuroscience research and clinical applications[2]. Automatic classification of tissues of brain into major type: gray white matter (WM), matter (GM) and cerebrospinal fluid (CSF) are used in various clinical applications to identify several brain diseases including Alzheimer's diseases, Aphasia, Multiple Sclerosis, Encephalopathy and Epilepsy[3]. Hence, precise disease investigation process and proper treatment preparation depends largely on the outcome of segmentation algorithm employed[4].

Absolute segmentation is a very difficult task because of the tissue mixture, which is caused by non-uniform field, partial volume effect (PV) effects, noise, and magnetic field non-uniformities[2][5]. Brain tissue classification from magnetic resonance imaging (MRI) T1-weighted (T1W) is of becomes vital need in most neuroscience application.

Moreover, precise brain tissue classification is quite a challenging task because of the intensity profiles of non-uniformity in tissue caused by differences in acquisition protocols, models of the scanner and age. Furthermore, many algorithms predict healthy state from anatomy and contradict pathology result in cases like hyper intensities in white matter (WMHs)[5], [6].

Brain tissue segmentation aids diagnosis and treatment but remains challenging due to image artifacts like unclear tissue boundaries from imaging limitations [7]. Current brain tissue classification algorithms typically use statistical modeling of voxel intensities, MRF-based spatial smoothing to correct intensity inhomogeneities, and probabilistic brain atlases. However, several factors still pose significant challenges to their effectiveness [8].

Markov random field (MRF) based algorithms have indicated strong capabilities in handling issues of noisy brain image classification compared to other algorithms[9]. In this work, a hidden Markov random field fitted with modified expectation maximisation algorithm is used for

neighbourhood correlation (addressing PV effect) and intensity inhomogeneity.

A. Magnetic Resonance Imaging in the Clinic

Magnetic resonance imaging (MRI) is a key non-invasive and non-ionizing tool for visualizing brain anatomy. The scanned area is divided into 3D voxels, each labeled based on anatomical structures using T1-weighted tissue classification. The main brain tissues are white matter (WM), gray matter (GM), and cerebrospinal fluid (CSF) [10], [11].

In T1-weighted images cerebrospinal fluid appears with dark gray colour, white matter with medium gray colour and gray matter with light gray colour[12]. Brain tissue classification typically focuses on WM, GM, and CSF, but voxels at tissue boundaries often present ambiguity. Fuzzy set segmentation addresses this by assigning membership values to multiple tissue types, allowing for more accurate feature estimation [8].

Brain tissue analysis plays a key role in diagnosing psychiatric and neurological disorders like schizophrenia, Alzheimer's, and bipolar disorder, and is also used in studies of brain development, aging, and surgical planning [10]. MRI holds strong potential as a biomarker for disease progression and treatment monitoring, relying on accurate brain tissue classification, with advancing MRI technology enabling faster 3D data acquisition, clinicians can use segmented brain data alongside age-adjusted norms for enhanced diagnosis[10].

B. Existing Brain Tissue Classification Methods

Several methods have been developed for brain tissue classification, each with its strengths and limitations. Manual classification, carried out by experienced professionals such as radiologists and anatomists, involves manually labeling pixels of similar intensities, but it is time-consuming,

subjective, and affected by factors like poor contrast and complex imaging techniques[4], [13]. Region-based methods rely on intensity homogeneity and are effective in handling shape and boundary detection using T1- or T2-weighted MR images. However, they are sensitive to noise, intensity inhomogeneity, and require post-processing due to weak edges[4], [14]. Thresholding methods, including fixed and adaptive techniques, are simple and computationally efficient but often fail in noisy or multimodal images. Clustering-based methods group pixels based on similarity measures and typically use T1-weighted images. Mixture models can handle intensity variation and spatial regularization but lack spatial context among voxels, leading to local optima[4], [15]. Feature extraction and classification methods apply machine learning algorithms such as support vector machine (SVM), artificial neural network (ANN), K-Nearest Neighbors (KNN), and Self-Organizing Map (SOM) on extracted features[5], [16]. Clustering algorithms classify brain tissue by grouping pixels or voxels with similar intensity or structural features into clusters, typically representing gray matter, white matter, and cerebrospinal fluid. Techniques like K-means, Fuzzy C-means, and SOM are commonly used in MRI analysis to segment and study brain structures. However, it is sensitive to noise and performs poorly on overlapping tissue[16], [17], [18]. These are efficient and capture local properties but are sensitive to heterogeneous intensities, noise, and unclear tissue boundaries[4] see Table 1 for some related literature. Hidden Markov Random Field and Expectation Maximization (HMRF-EM) is a brain segmentation algorithm that combines spatial context (HMRF) with statistical modeling (EM) to classify brain tissues in MRI images. It models the spatial dependencies between neighboring pixels/voxels to improve segmentation accuracy. It has the strengths of noise reduction by considering neighborhood information, handles intensity inhomogeneity better than simple clustering and Enhances tissue boundary detection compared to non-spatial methods.

Table 1: Some Selected Work in the Literature of the State of the Art of Brain Tissue Segmentation

Method	Year	Input	Problem accounted	Reference
Clustering methods	2024	Comparing k-means (KM) and Fast fuzzy C-means (FFCM)	Evaluation of performance	[19]
Feature extraction	2016	Likelihood function	Intensity inhomogeneity and special location	[20]
Thresholding segmentation	2017	Post processing pipeline (TS-PP)	Improve performance	[21]
Barkerly wavelet transformation (BWT) and support vector machine (SVM)	2017	Handling multi-scan image acquisition	Tumour detection and feature extraction using biologically inspired BWT	[22]
Clustering technique	2018	Super-voxel and efficient ensemble-based clustering	Improve performance	[23]
Feature extraction	2018	Two steps: extraction of gray scale level co-occurrence metric (GLM) feature followed by morphological filtering	Noise removal	[24]
Feature base (random forest)	2020	Robust in multi-centre and multi-scan data	Data variation with age using T1-weighted MRI	[5]
Clustering technique based on particle swarm optimization (PSO) algorithm and hierarchical evolutionary (HEA algorithm)	2010	Combination of PSO and HEA	Improved performance	[25]

Clustering methods	2020	Super-voxel clustering with 3D description for brain tissue segmentation	Replace the traditional handling strategies of 2D with 3D data	[26]
Clustering	2020	Fully automatic modified fuzzy C-means (MFCM)	Reduce processing time	[27]
Graph-self-constructed and fusion network	2021a	Using multiple types of image features	Improve performance	[28]
Deep multi modal fusion	2021b	Multi modal fusion segmentation	Evaluation of performance	[29]
Contextual multiscale multilevel network (CMM-net)	2021	Use deep learning in biomedical image segmentation	Tool use for various medical image segmentation	[30]
Feature extraction	2021	Fully automated brain segmentation method based on sparse representation of DWI signals	Improve performance	[31]
Hidden Markov Random Field	2023	Maximization algorithm	Partial volume effect	[32]

II. METHODOLOGY

A. Materials

- **Hardware:** Laptop with 4.00 GB RAM, 1.10 GHz processor, 64-bit OS. **Software:** R: A programming language for statistical computation and image creation, downloaded from www.r-project.org.
- **Rtools (4.0.028):** Required for building R packages, downloaded and set as the working directory in RStudio.
- **RStudio (1.4.1717):** Integrated development environment for R[33].

B. Method:

The study follows a structured workflow (Figure1), from data import to algorithm performance evaluation, using the Hidden Markov Random Field fitted with Expectation-Maximization (HMRF-EM), Normal Mixture method fitted with expectation maximization (NMM-EM), and Hidden Normal Mixture method fitted with iterated conditional mode (HNMM-ICM) algorithms. The performance metrics are as follows:

- **Misclassification Rate (misclass):** Measures voxel segmentation accuracy against the original anatomical structure.
- **Mean Square Error (MSE):** Evaluates the algorithm’s ability to handle partial volume effects by comparing estimated and true tissue distributions.
- **Dice Similarity Measure (DSM):** Defined by:

$$DSM_{a,b}^t = \frac{2N_{a \cap b}^t}{N_a^{t^2} + N_b^{t^2}} \tag{1}$$

Where N_a^b and N_b^t are the number of voxels classified at tissue t by method a and b respectively, and $N_{a \cap b}^t$ is the number of voxels classified as tissue t by both methods a and b . The larger the DSM, the more similar the result from both methods

- **Confusion Table (conTable):** Assesses classification accuracy on a per-tissue basis.
- **Tissue Volume Error (rsevolume):** Quantifies differences between calculated and true tissue volumes.

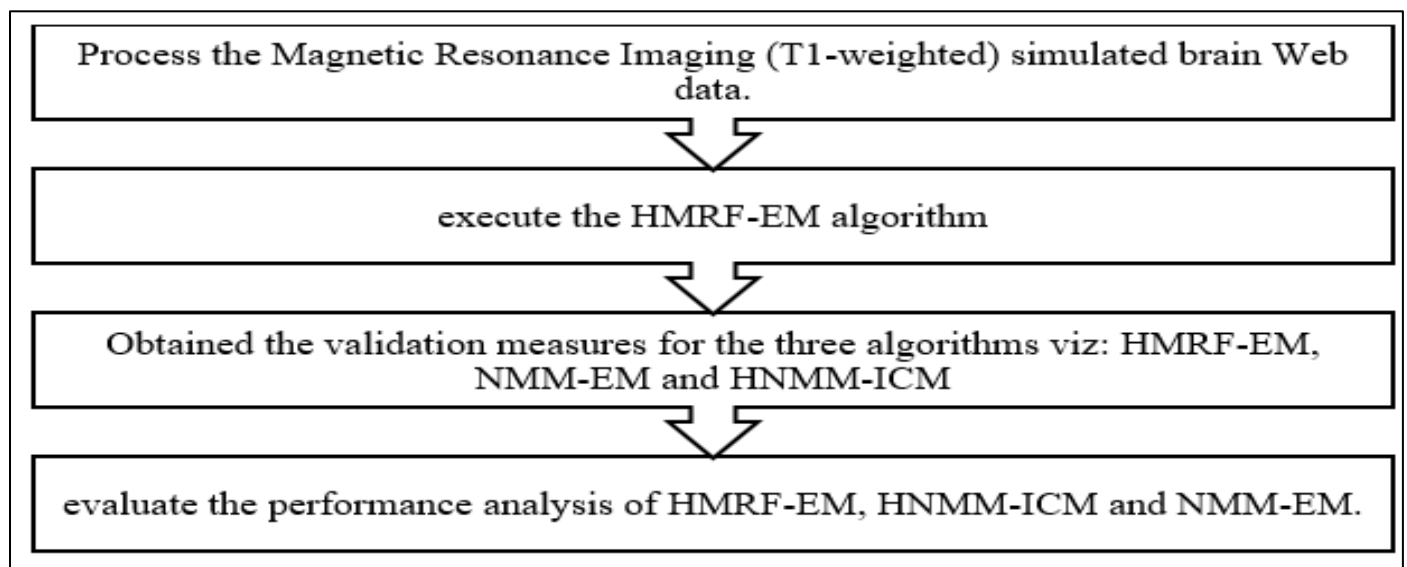


Fig 1: Schematic Representation of the Experimental Workflow, Illustrating the Sequential Steps Involved in Data Import, Preprocessing, Analysis, and Interpretation

HMRF is a Stochastic, undirected graphical model it works base on HMRF-EM algorithm shown in Figure 2. The segmentation process begins with an initial parameter set $\theta^{(0)}$. Using this, the likelihood distribution $P(y_i | X_i, \theta_{xi})$ is computed. Based on the current parameter set $\theta^{(t)}$, provisional

labels are estimated. The posterior distribution $P^{(t)}(l | y_i)$ is then calculated for all labels $l \in L$ and pixels y_i . These posterior probabilities are used to update the parameter set iteratively, refining the segmentation with each iteration.

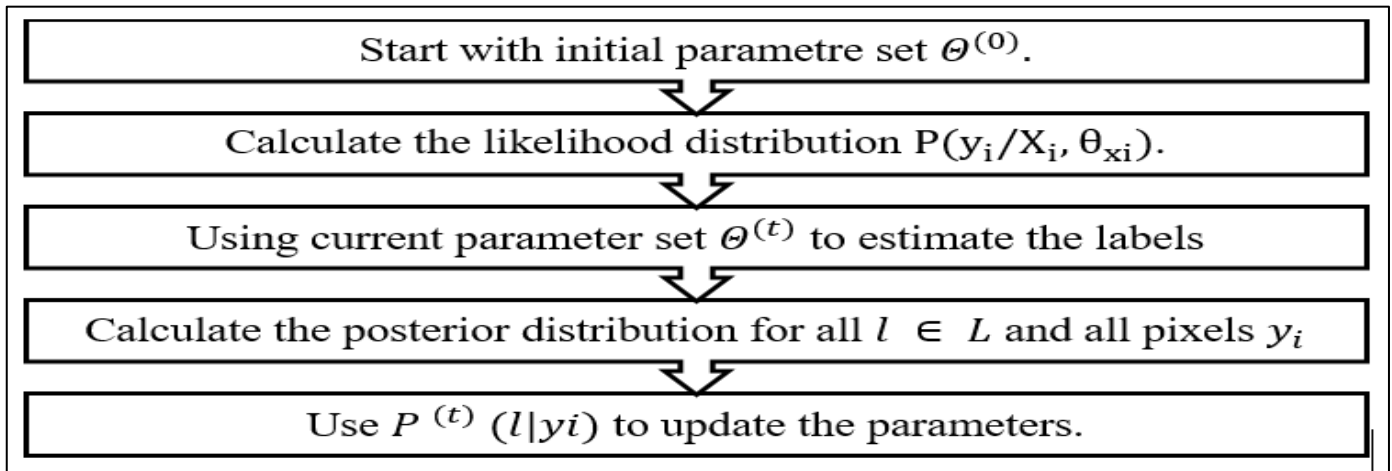
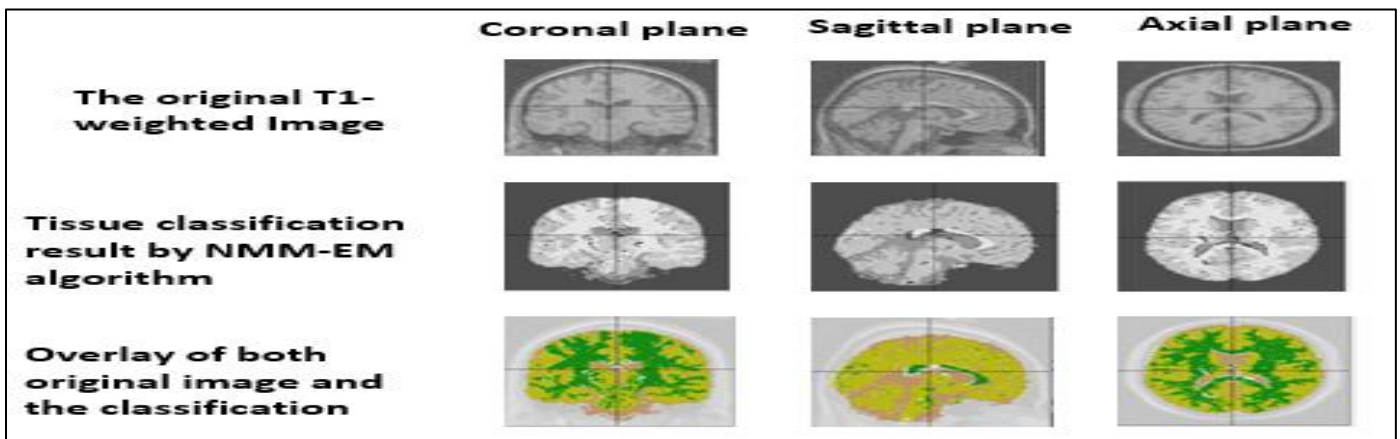


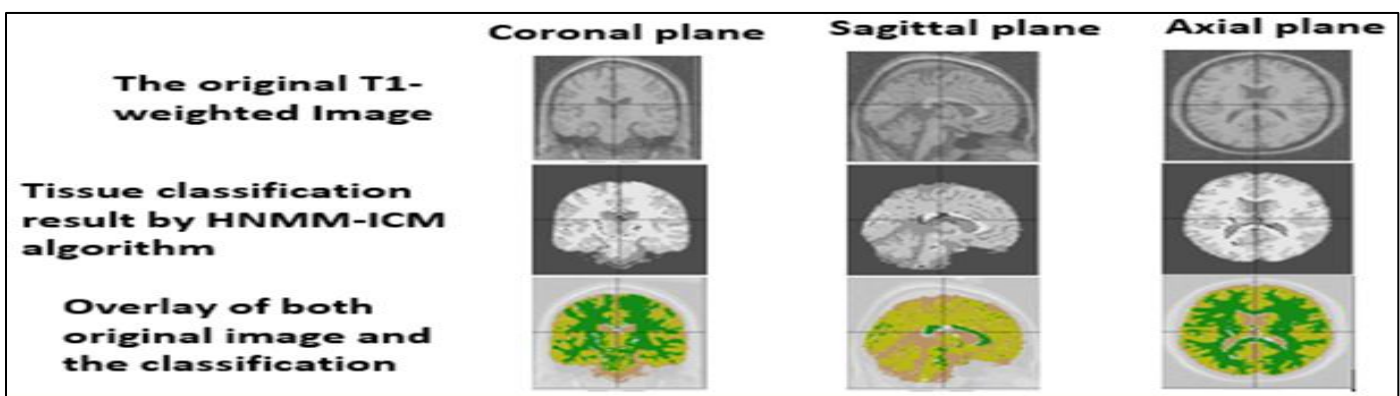
Fig 2: Schematic Representation of the HMRF-EM Algorithm, Illustrating the Iterative Process of Parameter Initialization, Likelihood Estimation, Label Inference, Posterior Computation, and Parameter Update for Brain Tissue Segmentation

III. RESULTS AND DISCUSSION

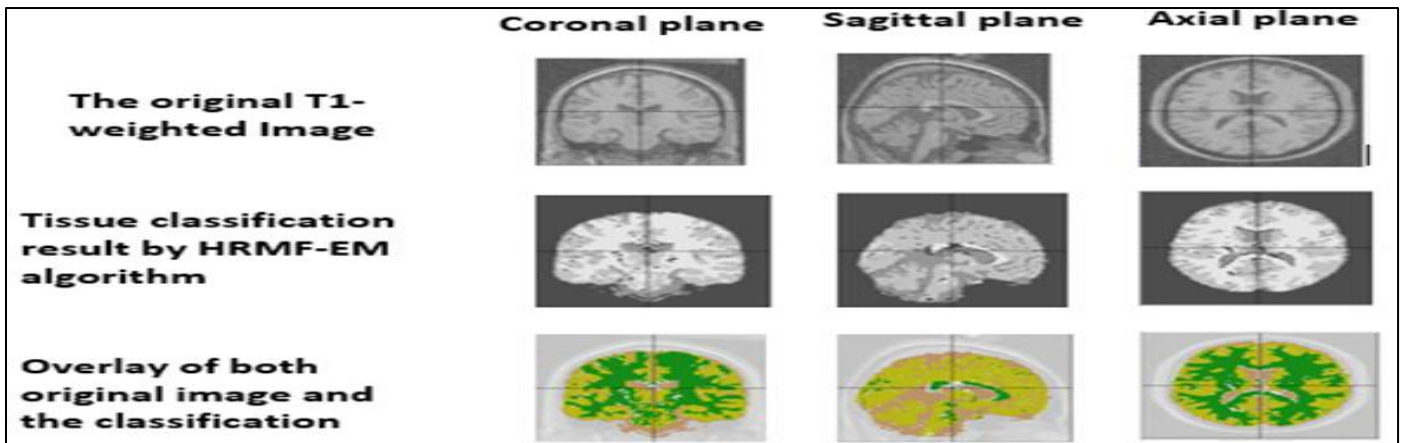
The study results are presented for the three MR brain tissue classification methods: HMRF-EM, NMM-EM, and HNMM-ICM. Results are organized as follows: Image plots using MISC3D, tkrplot (grayscale), and color plots. Density plots comparing predicted and actual data. Validation metrics: MSE, misclassification rate, DSM, confusion Table, and tissue volume error (rsevolume). Summary statistics Percentages for the three major brain tissue classifications.



(a)



(b)



(c)

Fig 3: (a) Original T1-Weighted Image, NMM-EM Classification Result, and Overlay. (b) Original T1-Weighted Image, HNMM-ICM Classification Result, and Overlay. (c) Original T1-Weighted Image, HMRM-EM Classification Result, and Overlay. In all (a), (b) and (c) White Matter Appears White, Gray Matter Light Gray, and Cerebrospinal Fluid Dark Gray, with Respective Overlay Colors as green, yellow-green, and Sandy Brown. Black Voxels Indicate Regions Outside the Brain

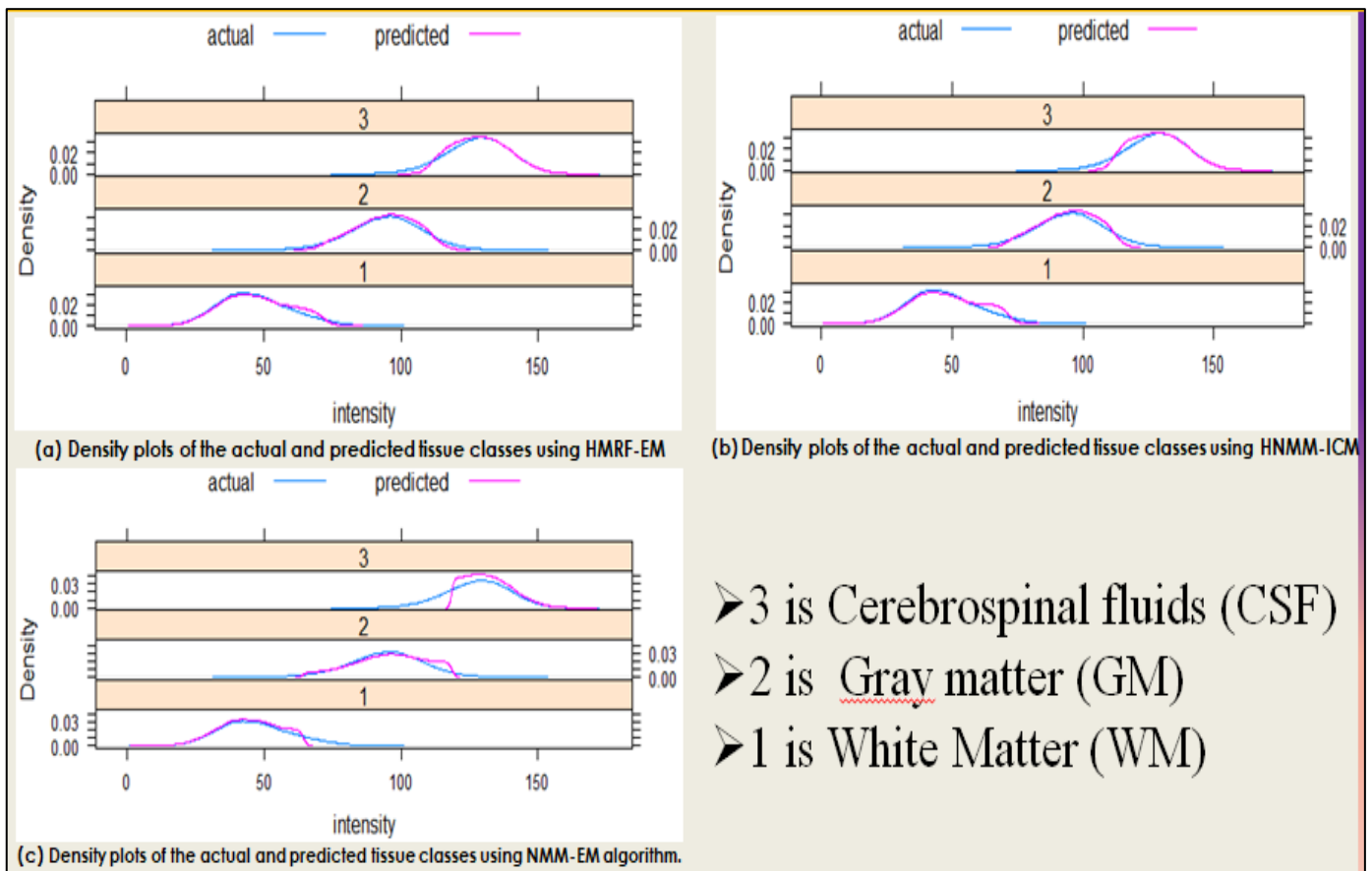


Fig 4: Density Plots of the Actual and Predicted Tissue Classes using (a) HMRM-EM, (b) HNMM-ICM and (c) NMM-EM Algorithms

Figure 3 presents the tissue segmentation results from the three methods: (a) NMM-EM, (b) HNMM-ICM, and (c) HMRM-EM. In each panel, the original T1-weighted image is displayed alongside the respective classification result and overlay, with white matter (WM) appearing white, gray matter (GM) light gray, and cerebrospinal fluid (CSF) dark gray. The overlay colors correspond to green for WM, yellow-green for GM, and sandy brown for CSF, while black voxels indicate regions outside the brain. Figure 4 compares

the actual and predicted tissue classes using density plots for each algorithm. (a) HMRM-EM shows the closest alignment with the actual data, with only minor differences in CSF and slight variations in GM and WM. In contrast, both (b) HNMM-ICM and especially (c) NMM-EM exhibit more significant mismatches, particularly in CSF segmentation. These findings highlight the superior performance of HMRM-EM in accurately classifying brain tissues.

Table 2: Misclassification Rate (Misclass) and Average Mean Square Error (MSE) for the Different Methods

Method	MSE	Misclass
HNMM-ICM	0.03023166	0.08898279
NMM-EM	0.03753136	0.11202600
HMRf-EM	0.02901258	0.08698963

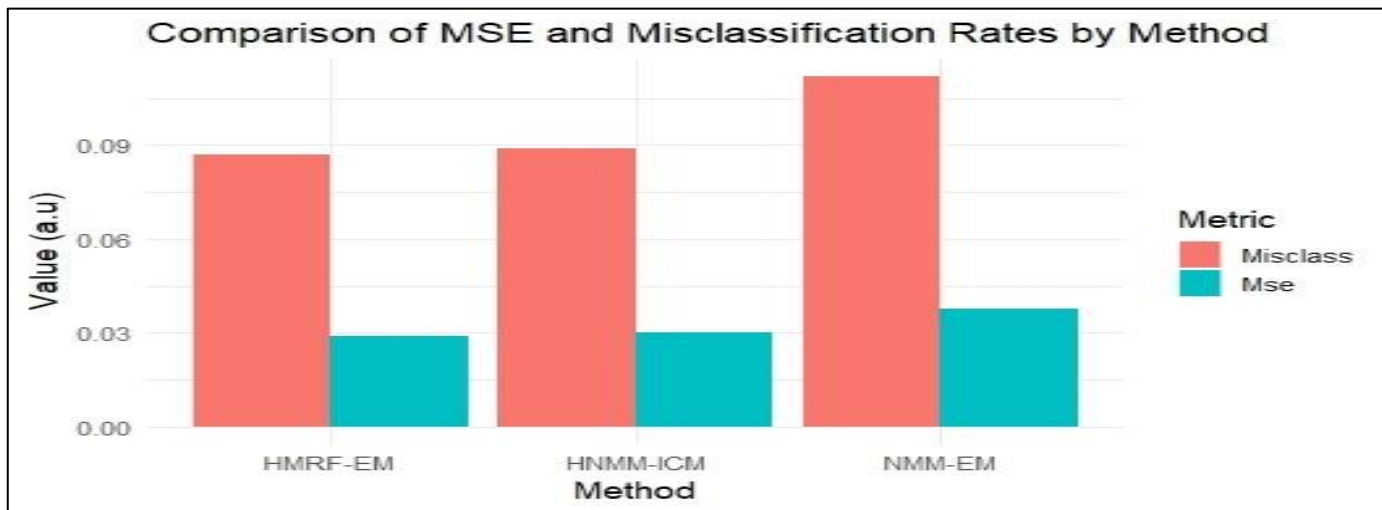


Fig 5: Comparison of Misclassification Rates and Mean Squared Error (MSE) Across the Three Methods

A comparison of misclassification rates and mean squared error (MSE) across the three methods reveals that the HMRf-EM algorithm outperforms both HNMM-ICM and NMM-EM, demonstrating superior segmentation accuracy

and robustness. Specifically, HMRf-EM achieves the lowest MSE and misclassification rate, indicating better overall performance in tissue segmentation see Table 2 and Figure 5.

Table 3: Tissue Volume Error (rse volume) for the Different Methods

Tissue /Method	HNMM-ICM	NMM-EM	HMRf-EM
CSF	0.06984997	0.0648337	0.057795173
GM	0.03455316	0.14343400	0.02458168
WM	0.014221461	0.16647681	0.006265323

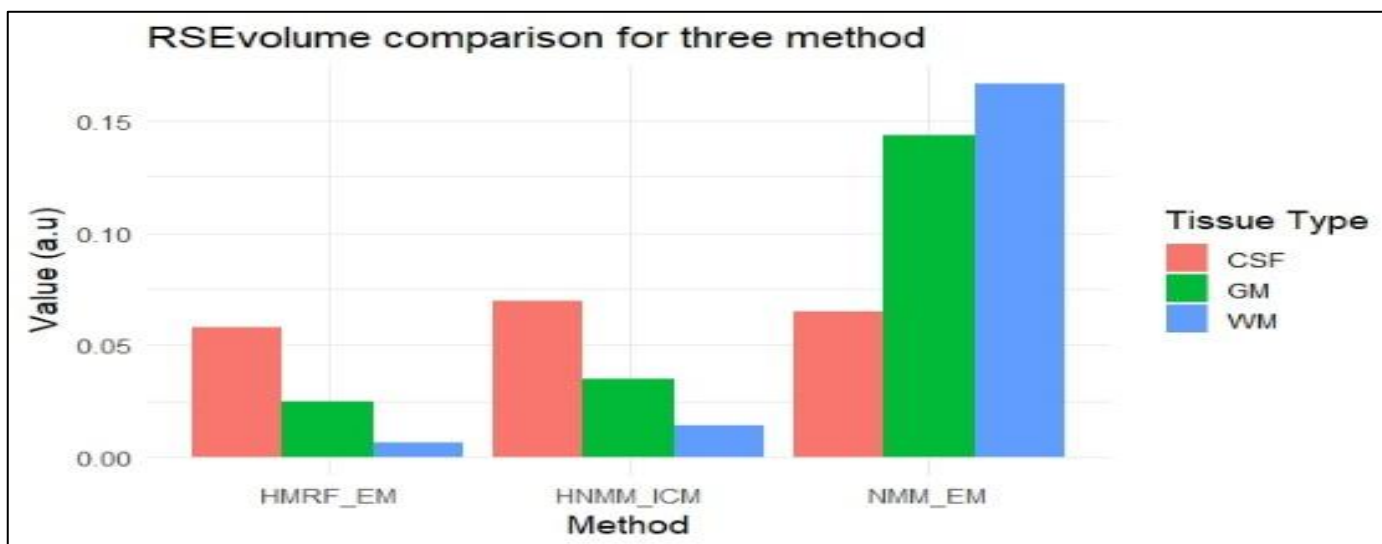


Fig 6: RSE Volume Comparison for Three Methods using the Tissue Type Based on Table 3, HMRf-EM Shows the Lowest Tissue Volume Error for CSF, GM, and WM, Outperforming NMM-EM and HNMM-ICM

The lower the value of the tissue volume error, the better the performance of an algorithm method and this indicates the probability of classifying voxel[34]. Based on the relative standard error (RSE) volume comparison presented in Table 3, the HMRf-EM algorithm exhibits the lowest tissue volume

estimation error across all tissue types: cerebrospinal fluid (CSF), gray matter (GM), and white matter (WM). This indicates that HMRf-EM provides more accurate tissue volume quantification compared to NMM-EM and HNMM-ICM see Figure 6.

Table 4: Dice Similarity Measures (DSM) for the Different Methods

Tissue /Method	HNMM-ICM	NMM-EM	HMRF-EM
CSF	0.9241746	0.9255292	0.9244405
GM	0.9060223	0.8915103	0.9085912
WM	0.9112816	0.8634850	0.9134111

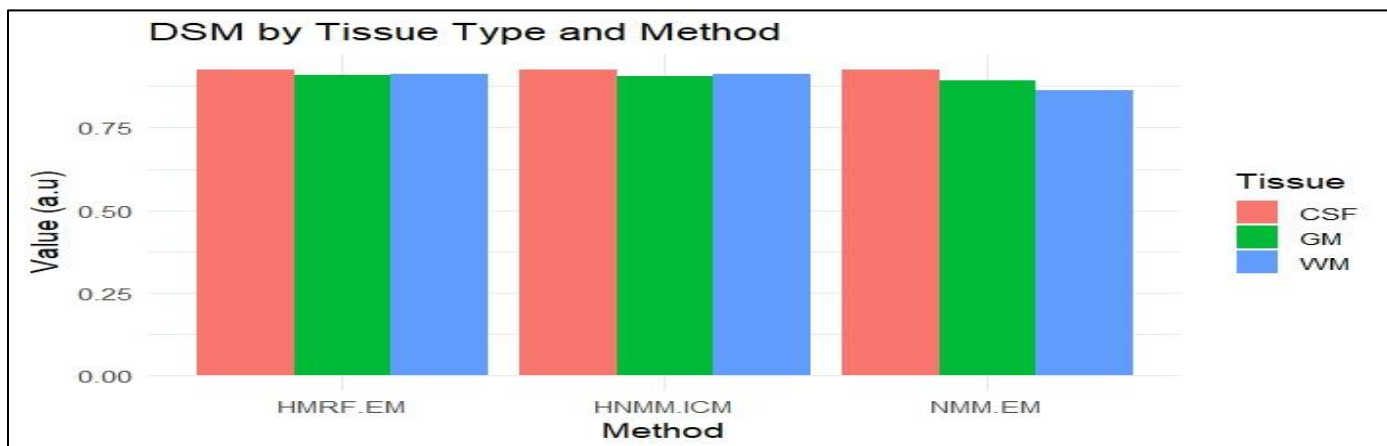


Fig 7: Dice Similarity Comparison for Three Methods using the Tissue Type

The dice similarity measure (DSM) as a statistical tool measures spatial overlapping, the higher the value for a particular tissue type the better the reproducibility of the method for DSM=0 indicates no overlapping, for 0<DSM<1 indicates partial overlapping and DSM=1 indicates complete overlapping [35]. The Dice similarity coefficient (DCM)

comparison across the three methods reveals that HMRF-EM outperforms both HNMM-ICM and NMM-EM in segmenting gray matter (GM) and white matter (WM), while NMM-EM slightly excels in cerebrospinal fluid (CSF) segmentation see Table 4 and Figure 7.

Table 5: Summary in Percentages of the Classification for the Different Methods

	Reference		
	WM/%	GM/%	CSF/%
HNMM-ICM	18	47	35
NMM-EM	16	55	29
HMRF-EM	18	47	35

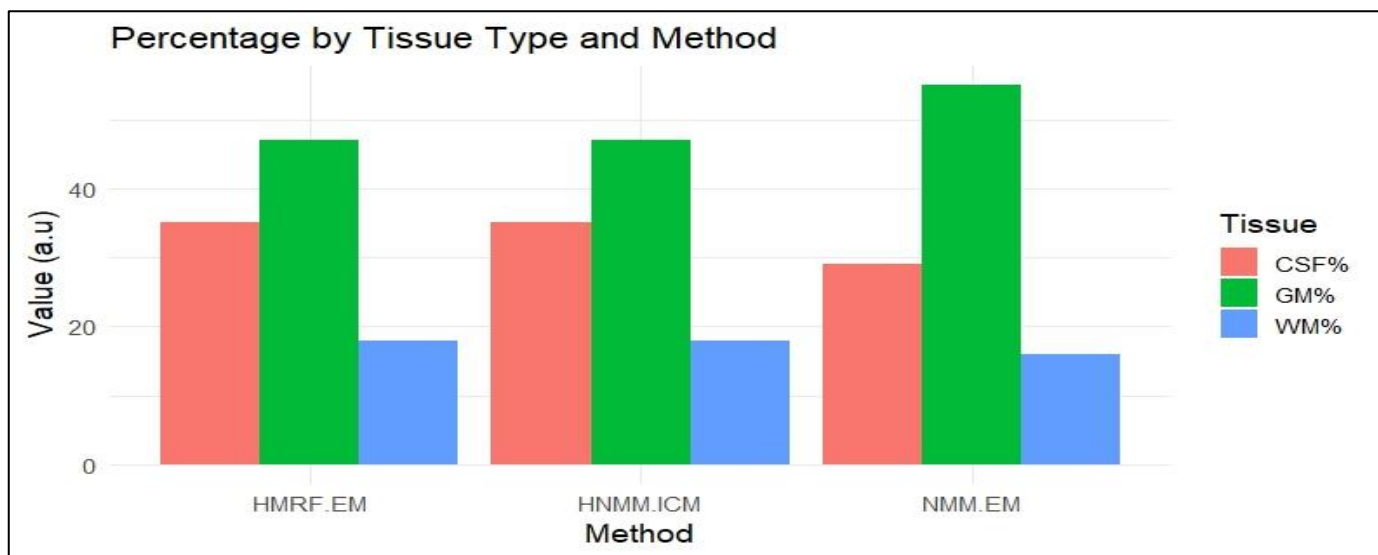


Fig 8: Summary of the Tissue Percentage Classification Comparison for Three Algorithms using CSF, GM, and WM

Table 5 presents the tissue volume percentage classification for CSF, GM, and WM across three algorithms. Both HNMM-ICM and HMRF-EM yield similar brain tissue volume percentages for all tissue types, with approximately 18% WM, 47% GM, and 35% CSF. In contrast, NMM-EM

shows significant deviations in tissue classification, with 16% WM, 55% GM, and 29% CSF. This highlights the consistency of HNMM-ICM and HMRF-EM in tissue volume estimation, while NMM-EM exhibits notable discrepancies see Figure 8.

Table 6 of confusion matrix for the tissue segmentation methods reveals HNMM-ICM and HMRF-EM demonstrate high accuracy in segmenting white matter (WM) and gray matter (GM), with minimal misclassification in CSF. In contrast, NMM-EM shows a noticeable discrepancy in

segmenting WM and GM, with higher misclassification rates, particularly for CSF. Overall, HMRF-EM provides a robust segmentation performance across all tissue types, achieving near-identical accuracy to HNMM-ICM, but with superior handling of GM and CSF.

Table 6: Confusion Table for the Different Methods for Brain Web Data

		Reference		
		WM	GM	CSF
HNMM-ICM	WM	0.9564514	0.03925961	0.0000000
	GM	0.0435486	0.89036938	0.08224165
	CSF	0.0000000	0.07037101	0.91775835
NMM-EM	WM	0.8961513	0.01397483	0.0000000
	GM	0.1038487	0.95544675	0.2083901
	CSF	0.0000000	0.03057842	0.7916099
HMRF-EM	WM	0.9511546	0.03691994	0.0000000
	GM	0.0488454	0.89742455	0.0837275
	CSF	0.0000000	0.06565552	0.9162725

IV. CONCLUSION

Brain tissue classification is vital for diagnosis, prognosis, and treatment planning, but clinical application remains challenging due to imaging artefacts like noise, intensity non-homogeneity, and abnormal tissue signals. Rather than replacing experts, classification methods are intended to support clinical decisions. This study presents a soft clustering approach using the Hidden Markov Random Field with Expectation Maximization (HMRF-EM) for brain tissue classification. The method successfully segmented white matter (WM), gray matter (GM), and cerebrospinal fluid (CSF) in 18%, 47%, and 35% of simulated brain datasets from BrainWeb. It accounted for the partial volume effect through a 3D six-neighbor model and addressed intensity non-homogeneity using adaptive lower potentials. The method also improves classification accuracy for detecting tumors or MS lesions in T1-weighted MR images. Integration into MRI systems could enhance diagnostic reports by revealing more anatomical and physiological details. Compared to the Normal Mixture Model EM (NMM-EM) and iterated conditional mode approach, the HMRF-EM algorithm at the pure voxel level outperformed in classifying major brain tissues.

REFERENCES

- [1]. J.-S. Long, G.-Z. Ma, E.-M. Song, and R.-C. Jin, "Learning U-Net Based Multi-Scale Features in Encoding-Decoding for MR Image Brain Tissue Segmentation," *Sensors*, vol. 21, no. 9, p. 3232, May 2021, doi: 10.3390/s21093232.
- [2]. Y. Kong, X. Chen, J. Wu, P. Zhang, Y. Chen, and H. Shu, "Automatic brain tissue segmentation based on graph filter," *BMC Med Imaging*, vol. 18, no. 1, p. 9, Dec. 2018, doi: 10.1186/s12880-018-0252-x.
- [3]. B. Jafrasteh, M. Lubián-Gutiérrez, S. P. Lubián-López, and I. Benavente-Fernández, "Enhanced Spatial Fuzzy C-Means Algorithm for Brain Tissue Segmentation in T1 Images," *Neuroinform*, vol. 22, no. 4, pp. 407–420, Apr. 2024, doi: 10.1007/s12021-024-09661-x.
- [4]. L. Dora, S. Agrawal, R. Panda, and A. Abraham, "State-of-the-Art Methods for Brain Tissue Segmentation: A Review," *IEEE Rev. Biomed. Eng.*, vol. 10, pp. 235–249, 2017, doi: 10.1109/RBME.2017.2715350.
- [5]. M. Dadar and D. L. Collins, "BISON: Brain tissue segmentation pipeline using T1 -weighted magnetic resonance images and a random forest classifier," *Magnetic Resonance in Med*, vol. 85, no. 4, pp. 1881–1894, Apr. 2021, doi: 10.1002/mrm.28547.
- [6]. V. M. Rao et al., "Improving across-dataset brain tissue segmentation for MRI imaging using transformer," *Front. Neuroimaging*, vol. 1, p. 1023481, Nov. 2022, doi: 10.3389/fnimg.2022.1023481.
- [7]. I. F. Almog et al., "Full-field swept-source optical coherence tomography and neural tissue classification for deep brain imaging," *Journal of Biophotonics*, vol. 13, no. 2, p. e201960083, Feb. 2020, doi: 10.1002/jbio.201960083.
- [8]. S. Awate, T. Tasdizen, N. Foster, and R. Whitaker, "Adaptive Markov modeling for mutual-information-based, unsupervised MRI brain-tissue classification," *Medical Image Analysis*, vol. 10, no. 5, pp. 726–739, Oct. 2006, doi: 10.1016/j.media.2006.07.002.
- [9]. C. Li, J. Sun, L. Liu, and V. Palade, "A hybrid framework for brain tissue segmentation in magnetic resonance images," *Int J Imaging Syst Tech*, vol. 31, no. 4, pp. 2305–2321, Dec. 2021, doi: 10.1002/ima.22637.
- [10]. D. Feng, L. Tierney, and V. Magnotta, "MRI Tissue Classification Using High-Resolution Bayesian Hidden Markov Normal Mixture Models," *Journal of the American Statistical Association*, vol. 107, no. 497, pp. 102–119, Mar. 2012, doi: 10.1198/jasa.2011.ap09529.
- [11]. S. D. Mikhaïlova, G. I. Storozhakov, S. I. Gukova, and T. M. Semushkina, "[Mechanism of the antiarrhythmic effect of laser irradiation]," *Biull Eksp Biol Med*, vol. 113, no. 5, pp. 460–462, May 1992.
- [12]. M. Tavakoli-Zaniani, Z. Sedighi-Maman, and M. H. Fazel Zarandi, "Segmentation of white matter, grey

- matter and cerebrospinal fluid from brain MR images using a modified FCM based on double estimation,” *Biomedical Signal Processing and Control*, vol. 68, p. 102615, Jul. 2021, doi: 10.1016/j.bspc.2021.102615.
- [13]. A. Fawzi, A. Achuthan, and B. Belaton, “Brain Image Segmentation in Recent Years: A Narrative Review,” *Brain Sci*, vol. 11, no. 8, p. 1055, Aug. 2021, doi: 10.3390/brainsci11081055.
- [14]. S. Yazdani, R. Yusof, A. Karimian, Y. Mitsukira, and A. Hematian, “Automatic Region-Based Brain Classification of MRI-T1 Data,” *PLoS ONE*, vol. 11, no. 4, p. e0151326, Apr. 2016, doi: 10.1371/journal.pone.0151326.
- [15]. Z. Bian, “MR brain tissue classification based on the spatial information enhanced Gaussian mixture model,” *Technol Health Care*, vol. 30, no. S1, pp. 81–89, 2022, doi: 10.3233/THC-228008.
- [16]. H. Tang, E. X. Wu, Q. Y. Ma, D. Gallagher, G. M. Perera, and T. Zhuang, “MRI brain image segmentation by multi-resolution edge detection and region selection,” *Computerized Medical Imaging and Graphics*, vol. 24, no. 6, pp. 349–357, Nov. 2000, doi: 10.1016/S0895-6111(00)00037-9.
- [17]. M. M and S. P, “MRI Brain Tumour Segmentation Using Hybrid Clustering and Classification by Back Propagation Algorithm,” *Asian Pac J Cancer Prev*, vol. 19, no. 11, pp. 3257–3263, Nov. 2018, doi: 10.31557/APJCP.2018.19.11.3257.
- [18]. M. Sucharitha and K. P. Geetha, “Brain tissue segmentation using fuzzy clustering techniques,” *THC*, vol. 23, no. 5, pp. 571–580, Sep. 2015, doi: 10.3233/THC-151012.
- [19]. “A comparison between the fuzzy C-means clustering algorithm and the K-mean clustering algorithm,” *Eng. Math. Lett.*, 2024, doi: 10.28919/eml/8403.
- [20]. P. Moeskops, M. A. Viergever, M. J. N. L. Benders, and I. Išgum, “Evaluation of an automatic brain segmentation method developed for neonates on adult MR brain images,” presented at the SPIE Medical Imaging, S. Ourselin and M. A. Styner, Eds., Orlando, Florida, United States, Mar. 2015, p. 941315. doi: 10.1117/12.2081833.
- [21]. P. Guo, “Brain tissue classification method for clinical decision-support systems,” *Engineering Applications of Artificial Intelligence*, vol. 64, pp. 232–241, Sep. 2017, doi: 10.1016/j.engappai.2017.05.015.
- [22]. N. B. Bahadure, A. K. Ray, and H. P. Thethi, “Image Analysis for MRI Based Brain Tumor Detection and Feature Extraction Using Biologically Inspired BWT and SVM,” *Int J Biomed Imaging*, vol. 2017, p. 9749108, 2017, doi: 10.1155/2017/9749108.
- [23]. H. Al-Dmour and A. Al-Ani, “A clustering fusion technique for MR brain tissue segmentation,” *Neurocomputing*, vol. 275, pp. 546–559, Jan. 2018, doi: 10.1016/j.neucom.2017.08.051.
- [24]. N. Varuna Shree and T. N. R. Kumar, “Identification and classification of brain tumor MRI images with feature extraction using DWT and probabilistic neural network,” *Brain Inform*, vol. 5, no. 1, pp. 23–30, Mar. 2018, doi: 10.1007/s40708-017-0075-5.
- [25]. M. Azarbad, A. Ebrahimzadeh, and A. Babajani-Feremi, “Brain tissue segmentation using an unsupervised clustering technique based on PSO algorithm,” in *2010 17th Iranian Conference of Biomedical Engineering (ICBME)*, Isfahan, Iran: IEEE, Nov. 2010, pp. 1–6. doi: 10.1109/ICBME.2010.5704938.
- [26]. Chien-shiung Wu College, Southeast University, Nanjing, China, Y. Liu, S. Du, and Y. Kong, “Supervoxel Clustering with a Novel 3D Descriptor for Brain Tissue Segmentation,” *IJMLC*, vol. 10, no. 3, pp. 501–506, May 2020, doi: 10.18178/ijmlc.2020.10.3.964.
- [27]. K. Thiruvankadam, K. Nagarajan, and S. Padmanaban, “An automatic self-initialized clustering method for brain tissue segmentation and pathology detection from magnetic resonance human head scans with graphics processing unit machine,” *Concurrency and Computation*, vol. 33, no. 6, p. e6084, Mar. 2021, doi: 10.1002/cpe.6084.
- [28]. F. Zhang et al., “Deep learning based segmentation of brain tissue from diffusion MRI,” *Neuroimage*, vol. 233, p. 117934, Jun. 2021, doi: 10.1016/j.neuroimage.2021.117934.
- [29]. Y. Zhang et al., “GSCFN: A graph self-construction and fusion network for semi-supervised brain tissue segmentation in MRI,” *Neurocomputing*, vol. 455, pp. 23–37, Sep. 2021, doi: 10.1016/j.neucom.2021.05.047.
- [30]. M. A. Al-Masni and D.-H. Kim, “CMM-Net: Contextual multi-scale multi-level network for efficient biomedical image segmentation,” *Sci Rep*, vol. 11, no. 1, p. 10191, May 2021, doi: 10.1038/s41598-021-89686-3.
- [31]. J. Wang, H. Cheng, and S. D. Newman, “Sparse representation of DWI images for fully automated brain tissue segmentation,” *J Neurosci Methods*, vol. 343, p. 108828, Sep. 2020, doi: 10.1016/j.jneumeth.2020.108828.
- [32]. M. Zitouni, M. Afif, and M. Zribi, “Tweedie hidden Markov random field and the expectation-method of moments and maximisation algorithm for brain MR image segmentation,” *Computer Methods in Biomechanics and Biomedical Engineering: Imaging & Visualization*, vol. 11, no. 1, pp. 67–79, Jan. 2023, doi: 10.1080/21681163.2022.2045225.
- [33]. I. Rizwan I Haque and J. Neubert, “Deep learning approaches to biomedical image segmentation,” *Informatics in Medicine Unlocked*, vol. 18, p. 100297, 2020, doi: 10.1016/j.imu.2020.100297.
- [34]. L. Lönn, G. Starck, M. Alpsten, S. Ekholm, and L. Sjöström, “Determination of tissue volumes. A comparison between CT and MR imaging,” *Acta Radiol*, vol. 40, no. 3, pp. 314–321, May 1999, doi: 10.3109/02841859909175560.
- [35]. K. H. Zou et al., “Statistical validation of image segmentation quality based on a spatial overlap index,” *Acad Radiol*, vol. 11, no. 2, pp. 178–189, Feb. 2004, doi: 10.1016/s1076-6332(03)00671-8.